eNeuro

Research Article: New Research | Sensory and Motor Systems

Newly Identified Electrically Coupled Neurons Support Development of the *Drosophila* Giant Fiber Model Circuit

Tyler Kennedy[1] and Kendal Broadie[1,2,3]

[1]*Department of Biological Sciences, Vanderbilt University and Medical Center, Nashville, TN 37235 USA*
[2]*Department of Cell and Developmental Biology, Vanderbilt University and Medical Center, Nashville, TN 37235 USA*
[3]*Vanderbilt Brain Institute, Vanderbilt University and Medical Center, Nashville, TN 37235 USA*

https://doi.org/10.1523/ENEURO.0346-18.2018

Received: 31 August 2018

Revised: 29 October 2018

Accepted: 12 November 2018

Published: 26 November 2018

Author contributions: T.K. and K.B. designed research; T.K. performed research; T.K. analyzed data; T.K. and K.B. wrote the paper.

Funding: http://doi.org/10.13039/100000065HHS | NIH | National Institute of Neurological Disorders and Stroke (NINDS)
NS092250

Funding: http://doi.org/10.13039/100000025HHS | NIH | National Institute of Mental Health (NIMH)
MH084989

Funding: http://doi.org/10.13039/100009633HHS | NIH | Eunice Kennedy Shriver National Institute of Child Health and Human Development (NICHD)
HD007502

The authors declare no competing financial interests.

Correspondence: Kendal Broadie, kendal.broadie@vanderbilt.edu

Cite as: eNeuro 2018; 10.1523/ENEURO.0346-18.2018

Newly Identified Electrically Coupled Neurons Support Development of the *Drosophila* Giant Fiber Model Circuit

Tyler Kennedy[1] and Kendal Broadie[1,2,3*]

[1]Department of Biological Sciences, [2]Department of Cell and Developmental Biology, [3]Vanderbilt Brain Institute, Vanderbilt University and Medical Center, Nashville, TN 37235 USA

Abbreviated Title: Expanded map of the *Drosophila* Giant Fiber Circuit

Author contributions: T.K. and K.B. designed research; T.K. performed research; T.K. analyzed data; T.K. and K.B. wrote the paper.

Acknowledgments: We are very grateful to the Bloomington *Drosophila* Stock Center (Indiana University, USA) for numerous transgenic lines used in this study, and also to Dr. Jonathan Bacon (University of Sussex, UK) for the kind gift of Shaking-B antibody. Imaging was performed with the Vanderbilt University Cell Imaging Shared Resource (supported by CA68485, DK20593). We appreciate the comments of Randall Golovin and Dr. James Sears on this manuscript. This work was supported by National Institutes of Health Grants MH084989 (to K.B.), and NS092250 and HD007502 (to T.K.).

Conflict of Interest: The authors declare no competing financial interests.

Number of Pages: 45

Number of Figures: 6

Number of Tables: 1

Number of Movies: 9

Significance Statement Word Count: 120

Abstract Word Count: 248

Introduction Word Count: 622

Discussion Word Count: 1925

***Correspondence:** kendal.broadie@vanderbilt.edu

Abstract

The *Drosophila* Giant Fiber (GF) escape circuit is an extensively studied model for neuron connectivity and function. Researchers have long taken advantage of the simple linear neuronal pathway, which begins at peripheral sensory modalities, travels through the central GF Interneuron (GFI) to motor neurons, and terminates on wing/leg muscles. This circuit is more complex than it seems however, as there exists a complex web of coupled neurons connected to the GFI, which widely innervate the thoracic ganglion. Here, we define four new neuron clusters dye-coupled to the central GFI, which we name GF Coupled (GFC) 1-4. We identify new transgenic Gal4 drivers that express specifically in these neurons, and map both neuronal architecture and synaptic polarity. GFC1-4 share a central site of GFI connectivity, the Inframedial Bridge (IB), where the neurons each form electrical synapses. Targeted apoptotic ablation of GFC1 reveals a key role for proper development of the GF circuit, including the maintenance of GFI connectivity with upstream and downstream synaptic partners. GFC1 ablation frequently results in loss of one GFI, which is always compensated for by contralateral innervation from a branch of the persisting GFI axon. Overall, this work reveals extensively coupled interconnectivity within the GF circuit, and the requirement of coupled neurons for circuit development. Identification of this large population of electrically-coupled neurons in this classic model, and the ability to genetically manipulate these electrically synapsed neurons, expands the GF system capabilities for the nuanced, sophisticated circuit dissection necessary for deeper investigations into brain formation.

Significance Statement

Genetic model neural circuits with individually identifiable neurons help us understand how nervous systems wire together during development, and then operate through coordinated chemical and electrical signaling. The *Drosophila* Giant Fiber circuit has long served as such a model, due to large neuron size, genetic malleability and easily visualized behavioral output: a jump in response to a threat. This study unveils new members of this circuit, all of which synapse with the circuit at one site on the central Giant Fiber Interneuron. We use new tools to identify and transgenically manipulate these neurons and show that these neurons are required for proper circuit development. This study provides a detailed circuit map for further dissection of neuronal connectivity and electrically-coupled communication.

Introduction

The *Drosophila* Giant Fiber (GF) circuit is particularly suitable for single-neuron resolution neurodevelopmental studies for a number of reasons, all related to its role as an escape response circuit (Allen et al., 2006; Boerner and Godenschwege, 2011). The need for rapid signal conduction from the senses through brain to muscles promoted evolution of very large neurons throughout this circuit, facilitating their visualization and manipulation (Power, 1948; Borgen et al., 2017). This enlargement is most prominent in the long-distance Giant Fiber Interneuron (GFI), which consolidates sensory information in the brain and projects through the neck into the thoracic ganglion (TG) via giant axons (Allen et al., 1998; Pézier et al., 2014). To increase communication speed and fidelity between neurons, the GF circuitry uses mixed chemical and electrical synapses (Thomas and Wyman, 1984; Blagburn et al., 1999; Fayyazuddin et al., 2006). These electrical synapses, composed of the Shaking-B innexin, can pass small tracer dyes to identify coupled partner neurons (Phelan et al., 1996).

The GF circuit targets two large muscle sets used for rapid escape behavior, the Tergotrochanteral Muscle (TTM), which controls the legs for jumping, and the Dorsal Longitudinal Muscle (DLM), which controls the wings (Tanouye and Wyman, 1980). The escape behavior is easily scored and muscles are accessible to electrophysiological recordings, providing two outlets to study whole circuit function (Martinez et al., 2007; Augustin et al., 2011; von Reyn et al., 2014). The GFI connects to the TTM via the Tergotrochanteral Motoneuron (TTMn) and to the DLM via the Peripherally Synapsing Interneuron (PSI), which in turn synapses onto the Dorsal Longitudinal Motoneuron (DLMn; Tanouye and Wyman, 1980; Allen et al., 2006). While the GF circuit is reported

to be quite simple, electrophoretic injections with small dyes make it clear that the GFI is actually part of a much larger circuit network of undescribed neurons (Boerner and Godenschwege, 2011; Enneking et al., 2013; Kennedy and Broadie, 2017).

This larger GF circuit should come as no surprise, as most classically studied circuits are continuously being updated to include new neurons, increasing appreciation of the complexity and interconnectivity within the brain (Lin et al., 2016; Talay et al., 2017; Zheng et al., 2017; Cande et al., 2018). Describing the wiring diagrams of classic circuits within model brains is important for understanding how local circuits accomplish processing tasks, while also overriding or promoting behaviors controlled by separated but interconnected circuits (Gaudry and Kristan, 2009; Stensmyr et al., 2012; von Reyn et al., 2014). More complex model circuits can better help answer questions about how circuits develop and evolve over time (Ward et al., 2015; Tosches, 2017). Combining GF circuit manipulability with the full complement of GFI-coupled neurons should enable robust new avenues for experimentation on how neurons select partners, determine synaptic strength and regulate neighboring circuits.

In this study, we use neurobiotin dye injection to map previously uncharacterized GF Coupled (GFC) neurons. We take advantage of the Flylight Gal4 library collection to identify transgenic drivers for the GFCs (Brand and Perrimon, 1993; Jenett et al., 2012). This approach defined four new GFI-coupled neuron clusters (GFC1-4) within the GF circuit, which we characterize for their architecture, neuronal polarity and synaptic connectivity. We show that the Inframedial Bridge (IB; Allen et al., 1998) is the GFI site where all the GFC neurons come together to synapse with the circuit. We ablate GF neurons by transgenic expression of the apoptotic Head Involution Defective (Hid)

protein (Zhou et al., 1997) to find that GFC1 and PSI are required for proper GFI development. We also find GFI axons always compensate for loss of their bilaterally symmetric partner through new contralateral innervation. Together, this work broadens the known GF circuit and opens new avenues for studying electrically-coupled circuit development, function and plasticity.

Materials and Methods

Drosophila Genetics

All animals were maintained on a standard cornmeal/agar/molasses *Drosophila* food in a 12-hour light:dark cycling incubator at 25ºC. Timed-lay eggs were collected for 2-3 days, and experimental animals were selected from rearing tubes 10-14 days later. The following *Drosophila* lines were used for genetic crosses: w^{1118} (RRID:BDSC_3605) | w^{1118}; P{GMR78A06-GAL4}attP2 (Jenett et al., 2012, RRID:BDSC_46999) | w^{1118}; P{GMR73C07-GAL4}attP2 (RRID:BDSC_46689) | w^{1118}; P{GMR24H07-GAL4}attP2 (RRID:BDSC_49317) | w^{1118}; P{GMR42A06-GAL4}attP2 (RRID:BDSC_41245) | w^{1118}; R10B11-p65.AD}attP40 (Dionne et al., 2018; RRID:BDSC_68807) | w^{1118}; P{GMR14A06-GAL4.DBD}attP2 (RRID:BDSC_68738) | w^{1118}, y^{1}; 10X UAS-*ivs-mCD8*::*GFP* attP40 (Pfeiffer et al., 2010) | UAS-*hid*.Z/CyO (Zhou et al., 1997; RRID:BDSC_65403) | w^{1118}; UAS-*DenMark*, UAS-*syt::GFP* (Zhang et al., 2002; Nicolai et al., 2010; RRID:BDSC_33064). Both females and males were used in this study, with sex-specific selection stated in figure legends. All genotypes were verified with visible markers.

Dye Iontophoresis

GFI dye injections were performed similar to the previously published methods (Boerner and Godenschwege, 2011; Kennedy and Broadie, 2017). Briefly; glass electrodes (Kwik-Fil Borosilicate glass 1B100F-4, World Precision Instruments) were pulled on a laser electrode puller (Model P-2000, Sutter Instrument Company) to 10MΩ resistance (3M KCl). Electrodes were filled with 0.25% TRITC-Dextran (10kDa, Life Technologies) and 7% neurobiotin (Vector Laboratories, RRID:AB_2313575) in ddH_2O. Filled electrodes were placed on a silver-chloride wire mounted on a PCS-5000 micromanipulator (Burleigh). Animals in physiological saline were cut along the dorsal midline to access the cervical connective (CC), at which electrodes were inserted into the GFI. A square-pulse stimulator (Grass S48, Astro-Med) provided 7.5 100ms pulses/second for 2 mins with the 20nA injected current monitored by an AxoClamp2B amplifier. A Digidata data acquisition system (1320A, Axon Instruments) was controlled with Clampex 9.2 software.

Confocal Imaging

Brains were fixed for 30 mins in 4% paraformaldehyde/sucrose (Electron Microscopy Services) in phosphate-buffered saline (PBS, pH 7.2, Life Technology) and then rinsed 3X with PBS, and blocked for 1 hr with 1% bovine serum albumin (BSA, Sigma-Aldrich) in PBST (PBS + 0.2% Triton X-100; Thermo Fisher Scientific). Labels were diluted in PBST with 0.2% BSA. The following labels were used: Streptavidin::Cy5 (1:20, Life Technology), rabbit anti-ShakB (1:250, Phelan et al., 1996), rabbit anti-GFP (1:2000; Abcam, RRID:AB_303395), FITC Goat anti-GFP (1:500; Abcam,

RRID:AB_305635), Rabbit anti-RFP (1:500; Rockland, RRID:AB_2209751), Alexa 488-conjugated donkey anti-goat (1:250; Thermo Fisher, RRID:AB_2534102), Alexa 488-conjugated donkey anti-rabbit (1:250; Thermo Fisher, RRID:AB_2556546), Alexa-568 conjugated donkey anti-rabbit (1:250; Thermo Fisher, RRID:AB_2534017), Alexa-647 conjugated donkey anti-rabbit (1:250; Thermo Fisher, RRID:AB_2536183), and Alexa-633 conjugated goat anti-rabbit (1:250; Thermo Fisher, RRID:AB_141419). Next, preparations were rinsed 3X for 30 mins in PBST, 1X in PBS, and then mounted on glass microscope slides (Probe On Plus 25 x 75 x 1.0mm, Thermo Fisher Scientific) in 2, 2'-Thiodiethanol (TDE, Sigma-Aldrich; Staudt et al., 2007). To prevent crushing, double-sided poster tape (Scotch) was placed on each side of the brains. Coverslips (No. 1.5H, Zeiss) were sealed with nail polish (Hard as Nails, Sally Hansen). Fluorescent images were collected using a ZEISS LSM 880 confocal microscope with an AiryScan module, which has increased lateral resolution (161nm) and signal-to-noise ratio (Sivaguru et al., 2016). Images show maximum Z-stack projections under standard confocal mode, unless otherwise noted in the figure legends.

Data Analyses

Data processing and image creation was done with FIJI software (version 2, RRID:SCR_002285; Schindelin et al., 2012; Schneider et al., 2012). Neuronal models and movies were created using Imaris (version 9.2, RRID:SCR_007370).

Results

The Giant Fiber Circuit Exhibits Extensive Dye-Coupled Connectivity

Small, gap junction permeable dyes used to study the Giant Fiber (GF) circuit have consistently revealed an extensive, but uncharacterized, network of dye-coupled neurons (Boerner and Godenschwege, 2011; Enneking et al., 2013; Kennedy and Broadie, 2017). In order to thoroughly study the architecture and properties of these neurons, we iontophoretically injected the Giant Fiber Interneuron (GFI) with the highly gap-junction permeable neurobiotin (NB) dye, and then labeled the brains post-hoc with a streptavidin-conjugated fluorophore (Huang et al., 1992). Consistent with previously published work, this intracellular dye injection reveals an extensive network of neurons dye-coupled to the GFI (Fig. 1). This dye-coupling is the direct result of gap junction connectivity, as eliminating gap junctions using *shaking-B* mutants (*shakB*^{2}) prevents all NB dye transfer (data not shown; Blagburn et al., 1999; Kennedy and Broadie, 2017). A summary of this newly identified GF circuitry is shown in Figure 1.

Although there are a large number of dye-labeled processes widely distributed throughout the thoracic ganglion (TG; Fig. 1*A*), all published GF circuit maps name only two GFI-coupled cells: 1) Tergotrochanteral Motoneuron (TTMn) and 2) Peripherally Synapsing Interneuron (PSI; Fig. 1*B*, 'old circuit map'). Here, we map and characterize all of the dye-coupled neurons whose projections we can trace back to an identifiable cell soma. We have named these neurons "Giant Fiber Coupled" (GFC) followed by an identifying number (Fig. 1*A*, *B*). In this study, we report the characterization of 4 neuron clusters (GFC1-4), each of which represents a bilaterally-symmetric set of 2-7 neurons (Fig. 1*B*, 'new circuit map'). The processes of these neurons contact the descending

GFI axons and reach into all three TG segments (TG1-3), but do not cross into the brain or abdominal ganglion (AG). To understand how the GFCs integrate into the GF circuit, we began by obtaining selective genetic access to these neurons.

Transgenic Gal4 Drivers for Newly Identified Giant Fiber Coupled Neurons

To accurately map and manipulate the separate GFC neuron populations, we set forth to identify Gal4 drivers with highly specific expression for each GFC using two approaches. First, we conducted an *in silico* screen through the entire Janelia FlyLight library, which includes lines generated from the Vienna Tiles project (9,436 lines; Jenett et al., 2012; Tirian and Dickson, 2017). Using images of the GFI dye-labeled circuit (Fig. 1*A*), we screened for matching GFP expression patterns (Fig. 2). We identified highly specific Gal4 drivers for GFC1 (78A06; Fig. 2*A*) and GFC2 (73C07; Fig. 2*B*), as well as less specific drivers for GFC3 and GFC4. Second, for cleaner GFC3 and GFC4 drivers, we used the recent automated Color-depth Maximum Intensity Projection (MIP) tool for the *Drosophila* transgenic database (Otsuna et al., 2018). Using the less specific driver lines as templates to search this library, we screened for specific Gal4 drivers for GFC3 and GFC4. This complementary approach uncovered a highly specific driver for GFC3 (24H07; Fig. 2*C*), and a combined driver for GFC3/4 (42A06; Fig. 2*D*). During our search with the MIP tool, we identified many additional GF circuit drivers, aside from the ones used in this study. We selected the cleanest drivers and report them in Table 1 for use in future experiments.

To confirm that the new Gal4 transgenic driver lines label the *bona fide* GFC components of the GF circuit, we crossed each Gal4 line with the UAS-*mCD8::GFP*

membrane reporter (Fig. 2, column 1) and injected the GFI with NB (Fig. 2, column 2). The merged images show perfect overlap between each transgenic driver line and the specified subset of the dye labeled neurons (Fig. 2, column 3). Cell bodies are strongly labeled in all cases (arrowheads), and individual neuronal processes of GFC1-4 can be traced for both the GFP and NB signals (arrows). However, in some cases, such as GFC2 (73C07-Gal4), the dye injection signal is much dimmer than for other neurons, such as GFC1 (78A06-Gal4). Each GFC cluster is schematically represented within the TG, with full color on one side (Fig. 1 color scheme) and dashed outlines on the other side, to show each individual GFC neuron as well as their bilaterally symmetrical pattern (Fig. 2, column 4). Using these Gal4-driven GFP expression patterns, we are able to map each GFC cluster within the TG.

Projection Architecture of GFC Neurons within the Thoracic Ganglion

GFC1 is comprised of 2 bilaterally symmetrical neurons on each side of TG2 (Fig. 2*A*). Each soma projects a process medially, which crosses the midline at the Inframedial Bridge (IB; Allen et al., 1998) and then splits, sending one branch anteriorly and one posteriorly. The anterior process travels halfway up TG1, then bends laterally and ventrally to terminate in the anterior corner of TG1, almost at the ventral-most point of the TG (Fig. 2*A*). This process extends several thin terminals, beginning in the same plane as the GFI bend. The posterior process splits halfway down TG2, just below the GFI bend. One branch proceeds laterally, then turns posteriorly towards the TG2 edge, with a ventral dive and several thin terminals, before terminating in the TG2 posterior lateral corner (Fig. 2*A*). The other process descends into TG3, bends inward towards

the midline, then laterally to the anterior edge. From here, the process projects posteriorly and ventrally to end in a similar fashion to the other two terminals (Fig. 2*A*). All three GFC1 projections appear to innervate the leg neuropils (Namiki et al., 2018).

The 7 bilaterally symmetric GFC2 neurons are largely restricted to TG2 (Fig. 2*B*). These cell bodies neighbor GFC1 and similarly project fasciculating processes medially. However, two-thirds of the way to the midline, the processes bend posteriorly and then laterally, to curve ventrally towards the lower edge of TG2 in the region of the GFI axon bend (Fig. 2*B*). The processes then curve anteriorly back towards the cell bodies, with a slight dorsal trajectory before termination, projecting several short, heavily-branched termini in anterior and posterior directions. Another process doubles back towards the posterior deflection, travels medially to the midline and then sends out two branches posteriorly (Fig. 2*B*). One curves ventrolaterally to terminate along the first ventral spiral, and the other travels dorsolaterally along the path of the original anterior process, terminating as it turns up towards the soma. There are two other processes that depart from the midline: one travels dorsally and slightly posteriorly before terminating, and one projects anteriorly and dorsolaterally to terminate in the lower central TG1 (Fig. 2*B*). These processes both appear to innervate the wing neuropils (Namiki et al., 2018).

GFC3 is comprised of 5 bilaterally symmetrical neurons with the cell bodies positioned dorsally in the posteriolateral corner of TG2 (Fig. 2*C*). These cells send out fasciculating processes that first proceed ventrally in a medial-anterior direction up to the central IB connection with the GFI. At the IB, extensive GFC3 branches are visible, extending laterally and dorsally, but no further in either anterior or ventral directions (Fig. 2*C*). These processes also track along the large terminal bend of the GFI axon.

Dorsal to the IB, the main GFC3 processes reverse course to travel posteriolaterally, while remaining ipsilateral to their cell bodies. The projection direction is ventral until TG3 is reached, at which point the processes move dorsally once again (Fig. 2*C*). These processes terminate near the anterior portion of TG3 within the leg neuropil, in a series of thin processes at approximately the same axial plane as the IB and GFI axonal bends (Fig. 2*C*). Of note, both GFC1 and GFC3 were unintentionally captured in a recent screen for descending neurons (Namiki et al., 2018).

The 4 bilaterally symmetric GFC4 neurons are largely restricted to TG1 (Fig. 2*D*). The GFC4 cell bodies lie in the TG1 dorsal lateroposterior corner. The GFC4 processes first fasciculate to project ventrally, then posterior-medially, running to the central IB (Fig. 2*D*). From the IB, the GFC4 processes then reverse course, remaining ipsilateral to their cell bodies as they project dorsally, back the way they came towards their cell bodies (Fig. 2*D*). When the GFC4 processes are directly below their cell bodies, they turn ventrally, and then travel towards the TG1 anteriolateral corner to terminate in long finger-like projects (Fig. 2*D*). Like the other GFCs, the GFC4 processes appear to innervate the leg neuropils (Namiki et al., 2018). Overall, these transgenic driver lines allow detailed analysis of GFC architecture, and provide highly specific genetic control over the GFC neurons. To determine how these neurons interact with the GF circuit, we next examined their contact points with the GFI.

The Inframedial Bridge Connectivity Site of GFI-GFC Intersection

GFC1-4 are all dye-coupled to GFI via direct or indirect gap junction connections (Fig. 1), and all of these neurons project to the central Inframedial Bridge (IB) to overlap

296 with the GFI (Fig. 2). The IB has been defined as a region proximal to the GFI lateral
297 axonal bend, where the GFI axon puts forth tufted projections and connects to the PSI
298 (Allen et al., 1998). We therefore hypothesized the IB is the primary site of GFI-GFC
299 connectivity. To determine the location of potential synaptic sites between the GFI and
300 GFCs, we injected the GFI with the large, non-permeant dye tetramethylrhodamine
301 (TRITC-dextran, 10 kDa; Boerner and Godenschwege, 2011; Enneking et al., 2013;
302 Kennedy and Broadie, 2017) for all the UAS-*mCD8::GFP* labeled GFC1-4 lines (Fig. 3).
303 We then assayed for overlap regions where GFC membrane signal (Fig. 3, column 1)
304 contacts the GFI TRITC signal (Fig. 3, column 2). Merging the two channels to create
305 static (Fig. 3, column 3) and dynamic (Movies 1-4) 3D reconstructions of the spatial
306 overlap provides clear identification of GFI-GFC contact points.
307 GFP and TRITC signals are color coded by depth to visualize the Z dimension
308 (FIJI plugin: Temporal-Color Code), with neurons proximal in Z space displaying the
309 same color (Fig. 3, columns 1, 2). Overlap between neurons is shown for GFCs (green)
310 and GFI (magenta; Fig. 3, column 3). The results show that GFC1 contacts the GFI only
311 at the IB with a simple crossing branch (Fig. 3*A*, arrows; Movie 1). GFC2-4 also contact
312 the GFI directly at the IB, but with a much higher level of complexity (Fig. 3*B-D*, arrows;
313 Movie 2-4). Further, GFC2 and 3 have processes that branch from the IB and overlap
314 the large terminal bend of the GFI axon (Fig. *3B,C*; arrowheads; Movies 2 and 3). This
315 is the first example, to our knowledge, of any contact along the GFI axonal bend other
316 than TTMn. We also observe a third contact point between GFI and GFC3. The GFI
317 axon bend occasionally extends small processes, which can contact GFC3 on
318 posteriorly descending processes (Fig. 3*C*, arrowhead; magnified in inset). As these

319 overlaps are likely sites for gap junction connectivity within the circuit, we investigated
320 these membrane contacts for electrical synapses.
321
322 **Shaking-B Gap Junction Synapses Between GFI and GFC Neurons**
323 The GF circuit is characterized by mixed chemical and electrical synapses
324 (Blagburn et al., 1999; Allen et al., 2006). To map GFI-GFC electrical synapses, we
325 labeled for the Shaking-B (ShakB) innexin, using an antibody recognizing the "N+16"
326 isoform present at GFI synapses (Phelan et al., 2008). Flies in which GFC1-4 neurons
327 are labeled with UAS-*mCD8::GFP* (Fig. 4, column 1, green) were GFI-injected with
328 TRITC (column 2, magenta) and co-labeled with ShakB antibody (column 3, cyan). All
329 three channels were modeled with 3D rendering software to visualize ShakB-positive
330 GFI-GFC contacts (Fig. 4, column 4; Movies 5-9). GFC1 (78A06-Gal4) exhibits a simple
331 arborization, with a process coming across the IB, and making a characteristic anterior-
332 posterior split (Fig. 4*A*; Movie 5). ShakB is clearly visible in the 3D models, localized
333 between the GFI and GFC1 as the process exits the IB (arrows and inset). GFC1
334 projects axons to all three TG segments, indicating that there is a set of outputs
335 triggered by the GFI escape response in parallel to TTM and DLM activation.
336 GFC2 neurons have a larger process field, forming a hemi-circle in front of the
337 GFI (Fig. 4*B;* Movie 6). Multiple ShakB electrical synapses clearly occur between the
338 GFI and GFC2, although due to the complexity of these connections, it is not possible to
339 determine if the GFI is contacting the GFC2 processes that come from the contra- or
340 ipsilateral sides of the TG, or both (Fig. 4*B*). GFC2 also contacts the GFI along the
341 distal axonal bend (Fig. 3*B*), so we also investigated these sites for ShakB co-

342 localization. The results show contact between the GFI and GFC2 near the tip of the
343 bend, however ShakB punctae are rarely seen co-localizing at these contacts (Fig. 4*C*;
344 Movie 7), suggesting these are primarily chemical synapse connections.

345 GFC3 has the most extensive IB contacts among all the GFCs, as well as broad
346 interactions with surrounding neurons (Fig. 4*D*; Movie 8). GFC3 contacts the GFI with
347 ShakB electrical synapses (arrows), but GFC3 branches extending beyond the IB are
348 mostly ShakB negative (Fig. 4*D*), indicating few electrical synapses. GFC3 contacts the
349 GFI axon bend even more extensively than GFC2, but similarly has a small number of
350 ShakB electrical synapse contacts (Fig. 4*E*; Movie 9). All images of GFI-GFC3 IB
351 contact sites exhibit ShakB-positive electrical synapses, but only one image of the GFI-
352 GFC3 axonal bend shows a synaptic connection (Fig. 4*E*, arrow). GFI axon bends are
353 presynaptic to the TTMn, with extensive ShakB electrical synapses (Phelan et al.,
354 2008), but it appears only a small portion of this gap junction connectivity is used for
355 GFC2 and 3, with the primary GFI-GFC electrical connections in the IB (Fig. 4*B*,*D*).
356 Without a GFC4-specific driver, we are unable to specifically test GFI-GFC4 ShakB
357 synaptic connections. To determine the direction of information flow across GFI-GFC
358 synapses, as well as connectivity in other regions of the TG, we next mapped the pre-
359 and postsynaptic neuronal polarity of GFC1-4 synapses.
360

361 **Pre- and Postsynaptic Polarity of Thoracic Ganglion GFC Neurons**

362 To investigate GFC postsynaptic domains, we used the UAS-*DenMark* dendrite
363 reporter, composed of the exogenous mouse ICAM5 dendritic protein fused to RFP
364 (Nicolai et al., 2010). For presynaptic labeling, we used the UAS-*synaptotagmin::GFP*

(Syt::GFP) reporter, composed of the Synaptotagmin1 (Syt1) integral synaptic vesicle protein fused to GFP (Zhang et al., 2002). In GFC1, the DenMark signal is absent from the finger-like projections at the process termini (Fig. 5*A*, column 1), and Syt::GFP is strongly present in a punctate array, indicating these processes are presynaptic sites (Fig. 5*A*, column 2). In contrast, DenMark strongly labels GFC1 within the IB (arrow), indicating this site is postsynaptic to the GFI (Fig. 5*A*, image column 3, top). The Syt::GFP signal is absent (Fig. 5*A*, image column 3, bottom), suggesting the IB site is solely for input. Together, these data indicate GFC1 neurons receive presynaptic input onto their dendrites at the IB and then project their contralateral axons for synaptic output into the leg neuropil (Namiki et al., 2018).

In contrast, GFC2 looped processes are strongly labeled by DenMark, including contacts at the GFI axon bend (Fig. 5*B*, column 1), with strongly co-localizing Syt::GFP (column 2). Only the dorsolaterally projecting processes in the wing neuropil display Syt::GFP without DenMark present. Similarly within the IB, DenMark and Syt::GFP again co-localize, although DenMark is at a low level (Fig. 5*B*, image column 3). Thus, GFC2 neurons appear to have many co-localized pre- and postsynaptic domains. Note that it is not possible to tell where in the loop GFC2 processes double back, and the pre- and postsynaptic compartments may be in separate, adjacent processes (Fig. 5*B*). Based on our ShakB findings (Fig. 4*B*), it is likely GFI and GFC2 directly synapse, but both appear presynaptic at the IB and they may also share postsynaptic targets that mediate GFI-GFC2 coupling. Another possibility is that GFI-GFC2 dye transfer does not occur at the IB, but instead they couple indirectly via an intermediary neuron. This could

387 explain why the GFC2 is relatively poorly labeled by NB dye injection into the GFI,
388 compared to other GFCs.

389 GFC3 has pre- and postsynaptic domains similar to GFC1 (Fig. 5*C*). The GFC3
390 long finger-like process projections in TG3 have very weak DenMark signal (column 1)
391 and very clear Syt::GFP punctae (column 2). Therefore, these sites are presumably
392 presynaptic in leg neuropil (Namiki et al., 2018). At the IB, GFC3 strongly expresses
393 DenMark (Fig. 5*C*, image column 3), which is thus postsynaptic. However, Denmark
394 expression expands beyond the IB to include GFC3 branches that parallel the GFI axon
395 bend and descending processes (Fig. 5*C*, arrowheads). Syt:GFP is undetectable at all
396 of these GFC3 sites, indicating they are solely postsynaptic (Fig. 5*C*, image column 3).
397 Surprisingly, DenMark/Syt::GFP expression is lethal with the 42A06-Gal4 driver, and we
398 were therefore unable to evaluate GFC4 pre- and postsynaptic domains. Based on
399 similarities to GFC3, we predict GFC4 has postsynaptic sites at the IB and presynaptic
400 sites in the TG1 leg neuropil. Overall, DenMark and Syt::GFP clearly distinguish pre-
401 and postsynaptic regions of all GFC neurons, except GFC2. As the GFCs are so
402 intimately interconnected with the GFI, we next tested if these coupled neurons play a
403 role in GF circuit development or maintenance.
404
405 **GFC Requirements for the Development of GF Circuit Architecture**
406 We used Gal4-targeted expression of the Head Involution Defective (Hid) protein
407 to drive apoptosis in GFC neurons, in an attempt to eliminate each GFC and study the
408 effects on the GF circuit architecture (Zhou et al., 1997; Muthukumar et al., 2014).
409 Unfortunately, all of the GFC drivers used above (Fig. 2) are lethal in combination with

410 UAS-*hid*. We repeated the study using split-Gal4 (spGal4) lines 10B11-AD ∩ 14A06-
411 DBD (Luan et al., 2006; Pfeiffer et al., 2010; Dionne et al., 2018) to eliminate the
412 apoptosis of off-target cells. These spGal4 lines were identified using the MIP search
413 tool, and were selected for their strong expression in GFC1 with minimal overlap in non-
414 specific neurons. This spGal4 combination expresses strongly in GFC1, but also in PSI,
415 as seen when crossed with UAS-*mCD8::GFP* (Fig. 6*A*, green) with injected TRITC
416 (magenta) to label the GFI. In the brain (Fig. 6*A*, top), only TRITC dye is present in the
417 GFI, where the GFI cell bodies (arrow) and their dendrites (arrowheads) reside.
418 Importantly, no mCD8::GFP is present in the GFI (Fig. 6*A*, green). Similarly, the Giant
419 Commissural Interneuron (GCI), which interconnects the GFIs, displays no mCD8::GFP.
420 In the TG, GFC1 (arrow) and PSI (arrowhead) express mCD8::GFP (Fig. 6*A*, bottom).
421 NB dye injection into GFI in a UAS-*hid*/+ control animal shows both GFIs labeled
422 in the brain (Fig. 6*B*, arrows). The GCI (arrowheads) interconnecting the GFI cell bodies
423 (Allen et al., 1998) is also dye labeled. In the TG, the intact dye-coupled GF circuit is
424 present in all UAS-*hid* /+ control animals (Fig. 6*B*, bottom). When the spGal4 driver is
425 crossed to UAS-*hid* and the GFI injected with NB, GFC1 is ablated in 18/20 animals
426 (90%); fully in 14/20, partially in 4/20 (Fig. 6*C*). Partial ablations are defined as several,
427 but not all, neurons within GFC1 clusters being killed. PSI is eliminated in 16/20 animals
428 (80%). Two animals had no visible cervical connective (CC) axons and could not be
429 injected for analysis. The ablation of coupled cells causes stronger dye labeling in the
430 persisting neurons, as expected due to the reduced volume of the GF circuit. As a
431 consequence, the standard 2-minute NB dye injection can cause lysis of the GF circuit,
432 and therefore injection times were reduced to $\leq$30 seconds for these ablation

433 experiments. This finding is similar to previous reports when GFI dye coupling is
434 eliminated through lack of interconnecting gap junctions (Kennedy and Broadie, 2017).

435 When testing the GF circuit for connectivity changes, we find GFC1/PSI ablation
436 causes a striking impact on GFI development (Fig. 6*C*). All control animals (UAS-*hid*/+,
437 n=21) display a completely normal dye-coupled GF circuit without detectable defects
438 (Fig. 6*B*). With targeted UAS-*hid* ablation (spGal4 10B11-AD ∩ 14A06-DBD>UAS-*hid*,
439 n=20 animals), in 9/14 animals (~65%) with complete GFC1 ablation (including 1 case
440 with the PSI present; Fig. 6*C*, arrowhead), one of the GFI neurons is completely absent
441 (Fig. 6*D,E*). In partial GFC1 ablation cases, only 1/4 animals (25%) lost a GFI. When a
442 GFI is lost, there is no visible dye within the neuron, including the soma and the axon
443 (Fig. 6*C*), and we only detect one axon traveling through the CC by light microscopy.
444 The remaining GFI always extends a compensating axon to the contralateral side
445 (10/10 animals; 100%) and forms a normal terminal axon bend (Fig. 6*C*, arrow).

446 Targeted UAS-*hid* expression is restricted to GFC1 and PS1, with no evidence of
447 either GFI or GCI expression. A full summary of the experimental results is compared
448 between UAS-*hid*/+ controls (n=21) and the spGal4 10B11-AD ∩ 14A06-DBD>UAS-*hid*
449 targeted ablation (n=20; Fig. 6*D,E*). Interestingly, in an animal with a fully intact GFC1
450 and only PSI ablation, both GFIs are present. In an animal with neither PSI nor GFC1
451 ablated, both GFIs are present (Fig. 6*D,E*). PSI ablation alone does not appear to be
452 responsible for GFI loss, as GFI loss occurs when GFC1 alone is missing, but not when
453 PSI alone is missing. We therefore conclude that GFC1 helps maintain GFI during GF
454 circuit development. Another interesting ablation result is the loss of GFI dye-coupling to
455 GCI in 5/10 animals (50%) where a GFI is lost (Fig. 6*C*). Surprisingly, this loss of GCI

456 also occurs in 2 animals where both GFIs are present; one with only GFC1 ablated, and
457 the other with only PSI ablated. These results suggest the GFC neurons, alongside the
458 classic GF circuit neurons, play an important role in neural circuit development.
459
460 **Discussion**
461 We describe here newly discovered neurons in the classic *Drosophila* Giant Fiber
462 (GF) neural circuit (Power, 1948; Sun and Wyman, 1997; Jacobs et al., 2000; Allen et
463 al., 2006) by characterizing four Giant Fiber Coupled (GFC) neuron clusters. We identify
464 specific transgenic drivers to both label and manipulate GFC1-4, and map neuronal
465 architecture and polarity. We show these neurons couple to the Giant Fiber Interneuron
466 (GFI) via ShakB N+16 innexin (Phelan et al., 2008) primarily at the central Inframedial
467 Bridge (IB; Allen et al., 1998), but also at the downstream axonal bend. Alongside the
468 already well-established benefits of this circuit, including the large cell size, genetic
469 malleability and accessible functional/behavioral readouts (Power, 1948; Tanouye and
470 Wyman, 1980; Phelan et al., 1996; Trimarchi et al., 1999), this expanded set of coupled
471 neurons can aid future experiments in neurodevelopment, such as the study of axonal
472 selection between multiple dendritic partners. This circuit map could be further refined
473 using advanced tools, such as MultiColor FlpOut (Nern et al., 2015), as was recently
474 accomplished for *Drosophila* brain descending neurons (Namiki et al., 2018).
475 This detailed circuit map is most useful for genetic analyses of electrical synapse
476 partner connectivity between individually defined neurons. The GFCs identified in this
477 study are comprised of 2-7 bilaterally symmetrical neurons clustered on each side of the
478 thoracic ganglion (TG) segments. Similar clusters of repeated neurons with apparent

connectivity redundancy have been recently identified in *Drosophila* brain descending neurons, where it is also unclear why neurons have such tightly overlapping projection patterns (Namiki et al., 2018). We have insufficient resolution to determine whether the GFC neurons truly are duplicates, or if they have distinct, proximally adjacent synaptic targets, like the closely overlapping Kenyon cells of the adult brain Mushroom Body (Crittenden et al., 1998). It has been proposed that neuron duplication may allow for a sliding scale of response within a circuit, whereby more neurons are activated to increase the strength of the response (Namiki et al., 2018). Alternatively, if the neurons contact similar proximal synaptic targets, their role may be to provide ultra-fine control of muscle movement in the GF circuit escape response (Namiki et al., 2018).

Complex leg and wing movements are thought to be controlled by extensive TG neural circuits, which are activated by a small number of descending neurons, including the GFI dedicated to rapid escape behavior (Cardona et al., 2009; Hsu and Bhandawat, 2016; Cande et al., 2018; Namiki et al., 2018). The roles of GFC neurons uncovered here have yet to be elucidated, although their electrical coupling to the GFI strongly suggests a close relationship to behaviors promoting or otherwise facilitating the rapid escape jump-and-flight response. Our preliminary attempts to optogenetically activate the GFC neurons through blue-light stimulation of Gal4-targeted ChR2-H134R (Nagel et al., 2005) or ChOP-XXL (Dawydow et al., 2014) channels did not produce behaviors. We suspect the stimulation paradigm was not strong enough, that appropriate sensory co-stimulation conditions may not have been provided (von Reyn et al., 2014), that behavioral scoring methods were not sensitive enough to detect subtle motor output

changes (Cande et al., 2018), or that these neurons modulate internal processes not directly manifest in rapid escape behavior (Joseph et al., 2017).

Based on the very recently proposed ventral nerve cord (VNC) regional map (Namiki et al., 2018), the most likely targets of the 4 GFCs identified here are the TG1-3 leg neuropils. GFC2 also appears to target the TG2 wing neuropil. Both leg and wing outputs are integral to the GF circuit escape response (von Reyn et al., 2014). GFC1 targets all three TG leg neuropil segments; GFC2 targets TG2; and GFC3 and GFC4 target TG3 and TG1, respectively. This extensive leg neuropil connectivity may regulate tension in the front and hind legs, allowing the central legs to execute a more effective escape jump (Trimarchi and Schneiderman, 1993; von Reyn et al., 2014; Namiki et al., 2018). In support of this hypothesis, our work indicates GFCs 1-3 are all directly gap junction coupled to the descending GFI, receiving input primarily at the IB, and thus share in the rapid conduction speed of the GF circuit (Phelan et al., 2008). Further, GFC3 neurons extend postsynaptic processes that parallel the PSI processes, indicating GFC3 may collect input from multiple neurons in the GF circuit.

Like the PSI, all 4 GFCs appear to synapse on their downstream targets via only chemical synapses, based on Syt::GFP synaptic vesicle marker and lack of ShakB electrical synapse labeling at GFC termini (Allen et al., 2006). It might appear possible that another innexin could mediate these GFC connections (Stebbings et al., 2002; Phelan, 2005); however, the complete absence of dye-coupling to neurons downstream of GFCs indicates electrical synapses are absent. In contrast to the other GFCs, GFC2 appears both pre- and postsynaptic at the IB connectivity hub, suggesting it may share postsynaptic partners with GFI, potentially including GFC1, 3, 4 and/or PSI. Given this

524 circuit connectivity, GFC2 may trigger the rapid escape jump reflex independently of the
525 GFI, in a parallel circuit output long speculated to exist, but not previously identified
526 (Trimarchi and Schneiderman, 1995; Fotowat et al., 2009). Indeed, GFC2 extends
527 presynaptic processes into the Tergotrochanteral Motoneuron dendritic field, thus
528 mimicking GFI connectivity (King and Wyman, 1980).

529 DenMark and Syt::GFP reporters are extremely useful in defining neuron polarity
530 (Zhang et al., 2002; Nicolai et al., 2010; Bidaye et al., 2014; Frank et al., 2015), but they
531 have limitations that can make interpretation difficult. Both reporters preferentially mark
532 appropriate synaptic regions, but can mis-localize due to transgenic overexpression
533 (Chen et al., 2014; Kanca et al., 2017). A likely example here is dim DenMark signal
534 near bright Syt::GFP punctae (Fig. 5*C*). DenMark signal-to-noise is much worse than
535 the IB labeling, while Syt::GFP signal-to-noise is much stronger; hence our conclusion
536 this region is presynaptic. A more problematic example may be the DenMark/Syt::GFP
537 overlap in GFC2 (Fig. 5*B*). This labeling likely shows adjacent pre- and postsynaptic
538 processes, which we cannot distinguish; although shared compartments have been
539 reported in Mushroom Body Kenyon cells (Christiansen et al., 2011; Zheng et al., 2018).
540 It is also worth noting the 73C07-Gal4 line for GFC2 is the strongest driver employed
541 and may cause DenMark or Syt::GFP mis-localization via transgenic overexpression
542 (Chen et al., 2014; Kanca et al., 2017). The 42A06-Gal4 driver for GFC3/4 is lethal with
543 UAS-*DenMark*, *syt::GFP*, showing these markers can also have detrimental effects.

544 Our targeted ablation studies indicate a role for GFCs in GF circuit development,
545 and demonstrate the ability of the circuit to compensate for the loss of a GFI, much like
546 ocular dominance columns in Hubel and Wiesel's classic work (Hubel and Wiesel, 1970;

Hubel et al., 1977). PSI ablation does not appear to be responsible for the GFI loss, based on the fact that GFIs are present when PSI alone is ablated, and GFIs are lost only when GFC1 is ablated. Another impact of ablation is lost GCI coupling when a GFI, GFC1 or PSI is removed. As GCI coupling loss occurs both when GFC1 alone is lost and when PSI alone is lost, it appears that complete GF circuit formation depends upon feedback from multiple circuit members (Kandler and Katz, 1995; Hanganu et al., 2009; Maher et al., 2009; Belousov and Fontes, 2013). This finding suggests neurons not directly coupled can feedback through an intermediary circuit neuron; an intriguing but poorly studied hypothesis (Kandler and Katz, 1995; Belousov and Fontes, 2013). We note that the TTMn only occasionally dye-couples with GFI, suggesting gap junction transitions between open and closed states could also contribute.

Previous studies have shown ablation of the GFI using neurotoxins, such as ricin (Smith et al., 1996), and have even found that single GFIs are lost at very low frequency in wildtype animals (Allen et al., 1998). In the latter case, the authors also found midline crossing of a compensatory contralateral process from the enduring GFI, as in our work. We hypothesize the GFI loss reported here results from lost GFI stabilization by GFC1 due to loss of trophic/synaptic signaling or physical contact (Gorin and Johnson, 1979; Pearson and Stoffler, 1992; Antonini and Stryker, 1993; Crowley et al., 1994; Uesaka, 2005; Gibson and Ma, 2011). Other GFI postsynaptic targets (PSI, TTMn, GFC2-4) presumably also participate in GFI stabilization, although Gal4 drivers tested thus far for these neurons have proved lethal in combination with UAS-*hid* (Zhou et al., 1997; Muthukumar et al., 2014). These animals die early in development, showing the need for spGal4 lines capable of avoiding off-target cells. Pursuing this phenotype with more

specific drivers and screening approaches could elucidate molecular mechanisms these neurons use to stabilize synaptic partners (Cohen-Cory, 2002).

Other methods shown to cause GFI axonal retraction and neuronal loss include blocking membrane endocytosis (e.g. using dominant negative *shibire*/Dynamin) and the overexpression of select transmembrane receptors, such as Semaphorin-1A (Godenschwege et al., 2002; Murphey, 2003; Godenschwege and Murphey, 2008). However, in these cases, GFI axon retraction is typically only to the IB, rather than beyond the CC, or causing complete cell loss. The molecular pathways responsible for these phenotypes may be shared with the axon retraction caused by loss of synaptic partners, with Highwire/MYCBP2, Wallenda/DLK and Basket/JNK as prime candidates (Ghosh et al., 2011; Borgen et al., 2017). While gap junctions play extensive roles in neuronal development (Elias and Kriegstein, 2008; Belousov and Fontes, 2013; Baker and Macagno, 2017), it is unlikely that GFI loss results from loss of electrical coupling only, as the total removal of gap junctions from the GFI does not cause axon retraction or neuronal cell death (Blagburn et al., 1999).

The GFI axon split across the midline in response to the absence of its partner is reminiscent of sensory neuron plasticity following input deprivation (Poirier et al., 2006; Collignon et al., 2009; Rabinowitch et al., 2016) and motor circuit development changes in response to lost motor neurons (Modney and Muller, 1994; Büschges et al., 2000). This corrective rewiring could stem from either normal pathfinding and synaptogenesis, or new repair pathways activated in response to unpartnered neurons. The axon split duplication with a GFI loss is different from the recent report on failed GFI pruning (Borgen et al., 2017), as the new GFI axon path is always a perfect mirror-image of the

normal axon bend, rather than an untrimmed posteriorly branched axon outgrowth. This new circuit rewiring model could be used in *Drosophila* genetic screens of GF circuit development (Mohr, 2014; Bassett et al., 2015; Heigwer et al., 2018) to help answer a number of important questions. Such work will be greatly aided by single-cell transgenic manipulation of pre- and postsynaptic neurons in the GF circuit.

In conclusion, we hope that the increase in manipulatable GFI coupled neurons reported here will further enhance this genetic model circuit. The GF circuit is ideally suited to query a wide range of important neurodevelopmental questions, including mechanisms of pathfinding, target recognition, synaptogenesis and stabilization during neural circuit assembly and maintenance. Although the GF circuit is rightly considered one of the most straightforward and accessible *Drosophila* circuits, the higher degree of connectivity revealed in this study indicates a greater complexity, which is amenable to answering more in-depth questions. The large number of inputs onto, and outputs from, this model circuit provides further evidence that even the most basic circuits are deeply interconnected with the rest of the brain circuitry. As the benefits of single-cell resolution studies cannot be overstated, we hope this enlarged GF circuit model, and the transgenic tools characterized here, will help form part of the underpinning for future work on neural circuit dynamics.

References

Allen MJ, Drummond JA, Moffat KG (1998) Development of the giant fiber neuron of Drosophila melanogaster. J Comp Neurol 397:519–531.

Allen MJ, Godenschwege TA, Tanouye MA, Phelan P (2006) Making an escape: development and function of the Drosophila giant fibre system. Semin Cell Dev Biol 17:31–41.

Antonini A, Stryker MP (1993) Rapid remodeling of axonal arbors in the visual cortex. Science 260:1819–1821.

Augustin H, Allen MJ, Partridge L (2011) Electrophysiological Recordings from the Giant Fiber Pathway of D. melanogaster. J Vis Exp.

Baker MW, Macagno ER (2017) Gap junction proteins and the wiring (Rewiring) of neuronal circuits. Dev Neurobiol 77:575–586.

Bassett AR, Kong L, Liu JL (2015) A Genome-Wide CRISPR Library for High-Throughput Genetic Screening in Drosophila Cells. J Genet Genomics 42:301–309.

Belousov AB, Fontes JD (2013) Neuronal gap junctions: Making and breaking connections during development and injury. Trends Neurosci 36:227–236.

Bidaye SS, Machacek C, Wu Y, Dickson BJ (2014) Neuronal control of Drosophila walking direction. Science 344:97–101.

Blagburn JM, Alexopoulos H, Davies JA, Bacon JP (1999) Null mutation in shaking-B eliminates electrical, but not chemical, synapses in the Drosophila giant fiber system: a structural study. J Comp Neurol 404:449–458.

Boerner J, Godenschwege TA (2011) Whole mount preparation of the adult Drosophila ventral nerve cord for giant fiber dye injection. J Vis Exp 52:3080.

634 Borgen M, Rowland K, Boerner J, Lloyd B, Khan A, Murphey R (2017) Axon
635 termination, pruning, and synaptogenesis in the giant fiber system of Drosophila
636 melanogaster is promoted by highwire. Genetics 205:1229–1245.
637 Brand AH, Perrimon N (1993) Targeted gene expression as a means of altering cell
638 fates and generating dominant phenotypes. Development 118:401–415.
639 Büschges A, Djokaj S, Bässler D, Bässler U, Rathmayer W (2000) Neuromuscular
640 plasticity in the locust after permanent removal of an excitatory motoneuron of the
641 extensor tibiae muscle. J Neurobiol 42:148–159.
642 Cande J, Berman GJ, Namiki S, Qiu J, Korff W, Card G, Shaevitz JW, Stern DL (2018)
643 Optogenetic dissection of descending behavioral control in Drosophila. Elife 7.
644 Cardona A, Larsen C, Hartenstein V (2009) Neuronal fiber tracts connecting the brain
645 and ventral nerve cord of the early Drosophila larva. J Comp Neurol 515:427–440.
646 Chen Y, Akin O, Nern A, Tsui CYK, Pecot MY, Zipursky SL (2014) Cell-type-specific
647 labeling of synapses in vivo through synaptic tagging with recombination. Neuron
648 81:280–293.
649 Christiansen F, Zube C, Andlauer TFM, Wichmann C, Fouquet W, Owald D, Mertel S,
650 Leiss F, Tavosanis G, Farca Luna AJ, Fiala A, Sigrist SJ (2011) Presynapses in
651 Kenyon Cell Dendrites in the Mushroom Body Calyx of Drosophila. J Neurosci
652 31:9696–9707.
653 Cohen-Cory S (2002) The developing synapse: Construction and modulation of synaptic
654 structures and circuits. Science 298:770–776.
655 Collignon O, Voss P, Lassonde M, Lepore F (2009) Cross-modal plasticity for the
656 spatial processing of sounds in visually deprived subjects. Exp Brain Res 192:343–

358.

Crittenden JR, Skoulakis EMC, Han K-A, Kalderon D, Davis RL (1998) Tripartite Mushroom Body Architecture Revealed by Antigenic Markers. Learn Mem 5:38–51.

Crowley C, Spencer SD, Nishimura MC, Chen KS, Pitts-Meek S, Armaninl MP, Ling LH, McMahon SB, Shelton DL, Levinson AD, Phillips HS (1994) Mice lacking nerve growth factor display perinatal loss of sensory and sympathetic neurons yet develop basal forebrain cholinergic neurons. Cell 76:1001–1011.

Dawydow A, Gueta R, Ljaschenko D, Ullrich S, Hermann M, Ehmann N, Gao S, Fiala A, Langenhan T, Nagel G, Kittel RJ (2014) Channelrhodopsin-2-XXL, a powerful optogenetic tool for low-light applications. Proc Natl Acad Sci U S A 111:13972–13977.

Dionne H, Hibbard KL, Cavallaro A, Kao JC, Rubin GM (2018) Genetic reagents for making split-GAL4 lines in Drosophila. Genetics 209:31–35.

Elias LAB, Kriegstein AR (2008) Gap junctions: multifaceted regulators of embryonic cortical development. Trends Neurosci 31:243–250.

Enneking E-M, Kudumala SR, Moreno E, Stephan R, Boerner J, Godenschwege TA, Pielage J (2013) Transsynaptic coordination of synaptic growth, function, and stability by the L1-type CAM Neuroglian. PLoS Biol 11:e1001537.

Fayyazuddin A, Zaheer MA, Hiesinger PR, Bellen HJ (2006) The nicotinic acetylcholine receptor Dalpha7 is required for an escape behavior in Drosophila. PLoS Biol 4.

Fotowat H, Fayyazuddin A, Bellen HJ, Gabbiani F (2009) A Novel Neuronal Pathway for Visually Guided Escape in Drosophila melanogaster. J Neurophysiol 102:875–885.

Frank DD, Jouandet GC, Kearney PJ, MacPherson LJ, Gallio M (2015) Temperature

representation in the Drosophila brain. Nature 519:358–361.

Gaudry Q, Kristan WB (2009) Behavioral choice by presynaptic inhibition of tactile sensory terminals. Nat Neurosci 12:1450–1457.

Ghosh AS, Wang B, Pozniak CD, Chen M, Watts RJ, Lewcock JW (2011) DLK induces developmental neuronal degeneration via selective regulation of proapoptotic JNK activity. J Cell Biol 194:751–764.

Gibson DA, Ma L (2011) Developmental regulation of axon branching in the vertebrate nervous system. Development 138:183–195.

Godenschwege T, Murphey R (2008) Genetic interaction of Neuroglian and Semaphorin1a during guidance and synapse formation. J Neurogenet 23:147–155.

Godenschwege TA, Hu H, Shan-Crofts X, Goodman CS, Murphey RK (2002) Bi-directional signaling by Semaphorin 1a during central synapse formation in Drosophila. Nat Neurosci 5:1294–1301.

Gorin PD, Johnson EM (1979) Experimental autoimmune model of nerve growth factor deprivation: effects on developing peripheral sympathetic and sensory neurons. Proc Natl Acad Sci U S A 76:5382–5386.

Hanganu IL, Okabe A, Lessmann V, Luhmann HJ (2009) Cellular mechanisms of subplate-driven and cholinergic input-dependent network activity in the neonatal rat somatosensory cortex. Cereb Cortex 19:89–105.

Heigwer F, Port F, Boutros M (2018) Rna interference (RNAi) screening in Drosophila. Genetics 208:853–874.

Hsu CT, Bhandawat V (2016) Organization of descending neurons in Drosophila melanogaster. Sci Rep 6.

703 Huang Q, Zhou D, DiFiglia M (1992) Neurobiotin(TM), a useful neuroanatomical tracer
704 for in vivo anterograde, retrograde and transneuronal tract-tracing and for in vitro
705 labeling of neurons. J Neurosci Methods 41:31–43.
706 Hubel DH, Wiesel TN (1970) The period of susceptibility to the physiological effects of
707 unilateral eye closure in kittens. J Physiol 206:419–436.
708 Hubel DH, Wiesel TN, LeVay S (1977) Plasticity of ocular dominance columns in
709 monkey striate cortex. Philos Trans R Soc Lond B Biol Sci 278:377–409.
710 Jacobs K, Todman MG, Allen MJ, Davies JA, Bacon JP (2000) Synaptogenesis in the
711 giant-fibre system of Drosophila: interaction of the giant fibre and its major
712 motorneuronal target. Development 127:5203–5212.
713 Jenett A et al. (2012) A gal4-driver line resource for Drosophila neurobiology. Cell Rep
714 2:991–1001.
715 Joseph RM, Sun JS, Tam E, Carlson JR (2017) A receptor and neuron that activate a
716 circuit limiting sucrose consumption. Elife 6.
717 Kanca O, Bellen HJ, Schnorrer F (2017) Gene tagging strategies to assess protein
718 expression, localization, and function in Drosophila. Genetics 207:389–412.
719 Kandler K, Katz LC (1995) Neuronal coupling and uncoupling in the developing nervous
720 system. Curr Opin Neurobiol 5:98–105.
721 Kennedy T, Broadie K (2017) Fragile X Mental Retardation Protein Restricts Small Dye
722 Iontophoresis Entry into Central Neurons. J Neurosci:0723-17.
723 King DG, Wyman RJ (1980) Anatomy of the giant fibre pathway in Drosophila. I. Three
724 thoracic components of the pathway. J Neurocytol 9:753–770.
725 Lin TY, Luo J, Shinomiya K, Ting CY, Lu Z, Meinertzhagen IA, Lee CH (2016) Mapping

chromatic pathways in the Drosophila visual system. J Comp Neurol 524:213–227.

Luan H, Peabody NC, Vinson CR, White BH (2006) Refined Spatial Manipulation of Neuronal Function by Combinatorial Restriction of Transgene Expression. Neuron 52:425–436.

Maher BJ, McGinley MJ, Westbrook GL (2009) Experience-dependent maturation of the glomerular microcircuit. Proc Natl Acad Sci 106:16865–16870.

Martinez VG, Javadi CS, Ngo E, Ngo L, Lagow RD, Zhang B (2007) Age-related changes in climbing behavior and neural circuit physiology in drosophila. Dev Neurobiol 67:778–791.

Modney B, Muller KJ (1994) Novel synapses compensate for a neuron ablated in embryos. Proc R Soc B Biol Sci 257:263–269.

Mohr SE (2014) RNAi screening in Drosophila cells and in vivo. Methods 68:82–88.

Murphey RK (2003) Targeted expression of shibirets and semaphorin 1a reveals critical periods for synapse formation in the giant fiber of Drosophila. Development 130:3671–3682.

Muthukumar AK, Stork T, Freeman MR (2014) Activity-dependent regulation of astrocyte GAT levels during synaptogenesis. Nat Neurosci 17:1340–1350.

Nagel G, Brauner M, Liewald JF, Adeishvili N, Bamberg E, Gottschalk A (2005) Light activation of Channelrhodopsin-2 in excitable cells of caenorhabditis elegans triggers rapid behavioral responses. Curr Biol.

Namiki S, Dickinson MH, Wong AM, Korff W, Card GM (2018) The functional organization of descending sensory-motor pathways in Drosophila. Elife 7:50.

Nern A, Pfeiffer BD, Rubin GM (2015) Optimized tools for multicolor stochastic labeling

749 reveal diverse stereotyped cell arrangements in the fly visual system. Proc Natl
750 Acad Sci 112:E2967–E2976.
751 Nicolai LJJ, Ramaekers A, Raemaekers T, Drozdzecki A, Mauss AS, Yan J, Landgraf
752 M, Annaert W, Hassan BA (2010) Genetically encoded dendritic marker sheds light
753 on neuronal connectivity in Drosophila. Proc Natl Acad Sci 107:20553–20558.
754 Otsuna H, Ito M, Kawase T (2018) Color depth MIP mask search: a new tool to expedite
755 Split-GAL4 creation. bioRxiv:318006.
756 Pearson HE, Stoffler DJ (1992) Retinal ganglion cell degeneration following loss of
757 postsynaptic target neurons in the dorsal lateral geniculate nucleus of the adult cat.
758 Exp Neurol 116:163–171.
759 Pézier A, Jezzini SH, Marie B, Blagburn JM (2014) Engrailed alters the specificity of
760 synaptic connections of Drosophila auditory neurons with the giant fiber. J Neurosci
761 34:11691–11704.
762 Pfeiffer BD, Ngo TTB, Hibbard KL, Murphy C, Jenett A, Truman JW, Rubin GM (2010)
763 Refinement of tools for targeted gene expression in Drosophila. Genetics 186:735–
764 755.
765 Phelan P (2005) Innexins: members of an evolutionarily conserved family of gap-
766 junction proteins. Biochim Biophys Acta 1711:225–245.
767 Phelan P, Bacon P, Moffat KG, Kane CJO, Davies JA (1996) Mutations in shaking-B
768 prevent electrical synapse formation in the Drosophila giant fiber system. J
769 Neurosci 6:1101–1113.
770 Phelan P, Goulding LA, Tam JLY, Allen MJ, Dawber RJ, Davies JA, Bacon JP (2008)
771 Molecular mechanism of rectification at identified electrical synapses in the

772 Drosophila giant fiber system. Curr Biol 18:1955–1960.
773 Poirier C, Collignon O, Scheiber C, Renier L, Vanlierde A, Tranduy D, Veraart C, De
774 Volder AG (2006) Auditory motion perception activates visual motion areas in early
775 blind subjects. Neuroimage 31:279–285.
776 Power ME (1948) The thoracico-abdominal nervous system of an adult insect,
777 Drosophila melanogaster. J Comp Neurol 88:347–409.
778 Rabinowitch I, Laurent P, Zhao B, Walker D, Beets I, Schoofs L, Bai J, Schafer WR,
779 Treinin M (2016) Neuropeptide-Driven Cross-Modal Plasticity following Sensory
780 Loss in Caenorhabditis elegans. PLoS Biol 14.
781 Schindelin J, Arganda-Carreras I, Frise E, Kaynig V, Longair M, Pietzsch T, Preibisch S,
782 Rueden C, Saalfeld S, Schmid B, Tinevez J-Y, White DJ, Hartenstein V, Eliceiri K,
783 Tomancak P, Cardona A (2012) Fiji: an open-source platform for biological-image
784 analysis. Nat Methods 9:676–682.
785 Schneider CA, Rasband WS, Eliceiri KW (2012) NIH Image to ImageJ: 25 years of
786 image analysis. Nat Methods 9:671–675.
787 Sivaguru M, Urban MA, Fried G, Wesseln CJ, Mander L, Punyasena SW (2016)
788 Comparative performance of airyscan and structured illumination superresolution
789 microscopy in the study of the surface texture and 3D shape of pollen. Microsc Res
790 Tech.
791 Smith HK, Roberts IJH, Allen MJ, Connolly JB, Moffat KG, O'Kane CJ (1996) Inducible
792 ternary control of transgene expression and cell ablation in Drosophila. Dev Genes
793 Evol 206:14–24.
794 Staudt T, Lang MC, Medda R, Engelhardt J, Hell SW (2007) 2,2 '-thiodiethanol: A new

795 water soluble mounting medium for high resolution optical microscopy. Microsc Res
796 Tech 70:1–9.
797 Stebbings LA, Todman MG, Phillips R, Greer CE, Tam J, Phelan P, Jacobs K, Bacon
798 JP, Davies JA (2002) Gap junctions in Drosophila: Developmental expression of
799 the entire innexin gene family. Mech Dev 113:197–205.
800 Stensmyr MC, Dweck HKM, Farhan A, Ibba I, Strutz A, Mukunda L, Linz J, Grabe V,
801 Steck K, Lavista-Llanos S, Wicher D, Sachse S, Knaden M, Becher PG, Seki Y,
802 Hansson BS (2012) A conserved dedicated olfactory circuit for detecting harmful
803 microbes in drosophila. Cell 151:1345–1357.
804 Sun Y, Wyman RJ (1997) Neurons of the Drosophila giant fiber system: I. Dorsal
805 longitudinal motor neurons. J Comp Neurol 387:157–166.
806 Talay M, Richman EB, Snell NJ, Hartmann GG, Fisher JD, Sorkaç A, Santoyo JF,
807 Chou-Freed C, Nair N, Johnson M, Szymanski JR, Barnea G (2017) Transsynaptic
808 Mapping of Second-Order Taste Neurons in Flies by trans-Tango. Neuron:1–13.
809 Tanouye MA, Wyman RJ (1980) Motor outputs of giant nerve fiber in Drosophila. J
810 Neurophysiol 44:405–421.
811 Thomas JB, Wyman RJ (1984) Mutations altering synaptic connectivity between
812 identified neurons in Drosophila. J Neurosci 4:530–538.
813 Tirian L, Dickson B (2017) The VT GAL4, LexA, and split-GAL4 driver line collections for
814 targeted expression in the Drosophila nervous system. bioRxiv:198648.
815 Tosches MA (2017) Developmental and genetic mechanisms of neural circuit evolution.
816 Dev Biol.
817 Trimarchi JR, Jin P, Murphey RK (1999) Controlling the motor neuron. Int Rev Neurobiol

43:241–264.

Trimarchi JR, Schneiderman a M (1995) Different neural pathways coordinate Drosophila flight initiations evoked by visual and olfactory stimuli. J Exp Biol 198:1099–1104.

Trimarchi JR, Schneiderman AM (1993) Giant fiber activation of an intrinsic muscle in the mesothoracic leg of Drosophila melanogaster. J Exp Biol 177:149–167.

Uesaka N (2005) Activity Dependence of Cortical Axon Branch Formation: A Morphological and Electrophysiological Study Using Organotypic Slice Cultures. J Neurosci 25:1–9.

von Reyn CR, Breads P, Peek MY, Zheng GZ, Williamson WR, Yee AL, Leonardo A, Card GM (2014) A spike-timing mechanism for action selection. Nat Neurosci 17:962–970.

Ward A, Hong W, Favaloro V, Luo L (2015) Toll Receptors Instruct Axon and Dendrite Targeting and Participate in Synaptic Partner Matching in a Drosophila Olfactory Circuit. Neuron 85:1013–1028.

Zhang YQ, Rodesch CK, Broadie K (2002) Living synaptic vesicle marker: Synaptotagmin-GFP. Genesis 34:142–145.

Zheng Z et al. (2017) A Complete Electron Microscopy Volume Of The Brain Of Adult Drosophila melanogaster. bioRxiv:140905.

Zheng Z, Lauritzen JS, Perlman E, Saalfeld S, Fetter RD, Bock Correspondence DD (2018) A Complete Electron Microscopy Volume of the Brain of Adult Drosophila melanogaster. Cell 174:1–14.

Zhou L, Schnitzler A, Agapite J, Schwartz LM, Steller H, Nambu JR (1997) Cooperative

functions of the reaper and head involution defective genes in the programmed cell death of Drosophila central nervous system midline cells. Proc Natl Acad Sci U S A 94:5131–5136.

Figure Legends

Figure 1: Giant Fiber Interneuron dye injection reveals coupled neurons

A, The Giant Fiber Interneuron (GFI) iontophoretically injected with neurobiotin (yellow) shows extensive dye-coupling to neurons in the thoracic ganglion (TG). The established GFI-coupled neurons are 1) the Peripherally Synapsing Interneuron (PSI; orange) and 2) the Tergotrochanteral Motoneuron (TTMn; red). The newly identified GFCs project into all three TG segments (TG1-3), but do not extend into the abdominal ganglia (AG). ***B,*** Left: The old GF circuit map showing both of the previously characterized GFI (green) dye-coupled neurons: PSI (orange) and TTMn (red). Right: The new GF circuit map with the addition of all the newly identified GFC neurons from this study: GFC1 (blue), GFC2 (purple), GFC3 (dark green) and GFC4 (yellow).

Figure 2: Transgenic Gal4 drivers for the newly identified GFC neurons

Gal4-driven expression of UAS-*mCD8::GFP* (green, column 1) overlapping with the GFI injection of neurobiotin dye (yellow, column 2) showing the identification of GFC drivers (merge, column 3). Arrows indicate processes with overlapping GFP and NB labeling, and arrowheads show the GFC cell bodies. The GFC neurons are drawn both in color (Fig. 1 color scheme) and perforated outlines to show their bilateral pattern (column 4). Thoracic ganglia (TG) segments are selected to best show GFC projection architecture. All injections were performed on females. ***A,*** 78A06-Gal4 labels GFC1. The driver strength is relatively weak, with a somewhat stochastic labeling of the GFC1 neurons. ***B,*** 73C07-Gal4 labels GFC2. This driver is moderately strong, but also labels other neurons. ***C,*** 24H07-Gal4 labels GFC3. This driver strength is moderate, with labeling of

other neurons. ***D,*** 42A06-GAL4 labels both GFC3 and GFC4 neurons. The driver is relatively weak, with stochastic labeling of GFC4 neurons.

Figure 3: The GFI interacts with the GFC neurons at the Inframedial Bridge

Gal4 lines driving UAS-*mCD8::GFP* (column 1) intersect with the GFI axon revealed by injection of tetramethylrhodamine (TRITC, column 2), at the GFI Inframedial Bridge (IB) and the GFI axonal bend (merge, column 3). The first 2 columns use depth color coding to represent Z-position within the TG, with more dorsal regions displaying cool colors and ventral regions displaying warm colors (see color scale bar in ***A***, column 2). Arrows indicate overlapping membrane contact between GFCs and GFI at the IB. Arrowheads indicate GFC contact at the GFI axon bend. All injected flies are female. ***A,*** GFC1 (78A06-Gal4) interacts with the GFI exclusively at the IB. ***B,*** GFC2 (73C07-Gal4) interacts with the GFI at the IB, and the GFI axonal bend. ***C,*** GFC3 (24H07-Gal4) interacts with the GFI extensively at the IB and the GFI axonal bend. The GFI also produces small side projections that contact GFC3 (inset, arrowheads). ***D,*** GFC4 (42A06-Gal4) interacts with the GFI at the IB.

Figure 4: GFCs form electrical synapses with the GFI at the Inframedial Bridge

Electrical synapses between GFI and GFC neurons are shown in Gal4-driven UAS-*mCD8::GFP* animals (green, column 1) with TRITC dye injection into the GFI (magenta, column 2), while co-labeling with the Shaking-B antibody (cyan, column 3). Images were taken using the microscope's AiryScan mode. The three merged channels (column 4) show the regions of shared ShakB contact between GFI-GFCs. Arrows indicate sites of

the GFI-GFC ShakB synaptic contacts (magnified in insets). All injected flies are female. ***A,*** GFC1 (78A06-Gal4) makes ShakB electrical synapse contacts with the GFI at the IB. ***B,*** GFC2 (73C07-Gal4) forms several ShakB electrical synapse contacts with the GFI. ***C,*** GFC2 (73C07-Gal4) contacts the GFI along the axonal bend. ***D,*** GFC3 (24H07-Gal4) contacts the GFI with multiple ShakB electrical synapses. ***E,*** GFC3 (24H07-Gal4) minimally contacts the GFI along the axonal bend (arrow).

Figure 5: Pre- and postsynaptic polarity of the newly identified GFC neurons

GFC neuronal polarity is shown using the dendrite/soma label DenMark (magenta) and the presynaptic label Synaptotagmin::GFP (Syt::GFP, green). Substacks of the regions of interest for each GFC are shown for DenMark (column 1) and Syt::GFP (column 2), with above and below paired comparisons (image column 3). Arrows indicate the position of the Inframedial Bridge (IB). GFC schematic representations are shown (center column), with regions of interest outlined in black boxes. ***A,*** GFC1 (78A06-Gal4) processes are labeled by presynaptic Syt::GFP in both TG1 (top) and TG2 (bottom) segments, while the IB is labeled by postsynaptic DenMark. ***B,*** GFC2 (73C07-Gal4) processes in TG2 (column 1) are co-labeled by both DenMark (column 1) and the Syt::GFP marker (column 2). The IB is labeled by presynaptic Syt::GFP, but also has the DenMark signal (column 4). ***C,*** GFC3 (24H07-Gal4) has punctate Syt::GFP within the finger-like processes in TG3 (column 2). The IB is labeled by DenMark, with no Syt::GFP marker (column 4). GFC3 processes along the GFI axonal bend also express the DenMark label (arrowheads).

Figure 6: GFC neurons support GF circuit architectural development

A, The GFI labeled by iontophoretically injected TRITC (magenta) reveals the soma (arrow) and dendritic branches (arrowheads) in the brain (top panel), and descending axon in thoracic ganglion (bottom panel). Split Gal4 (spGal4) 10B11-AD ∩ 14A06-DBD drives UAS-*mCD8::GFP* (green) in GFC1 (bottom, arrow) and PSI (bottom, arrowhead). ***B,*** Iontophoretic NB injection into the GFI (yellow) in the UAS-*hid*/+ control reveals the GFI (arrows) interconnected by the Giant Commissural Interneurons (GCI, arrowheads) in the brain (top panel), and normal dye-coupling in the thoracic ganglion (bottom panel). ***C,*** Driving UAS-*hid* with spGal4 10B11-AD ∩ 14A06-DBD results in the loss of GFC1 with occasional PSI survival (arrowhead). When GFC1 is ablated, the GCI labeling is often lost (top), one of the GFI axons is typically absent, and the remaining GFI axon always extends a compensatory contralateral axon projection (arrow). All NB injections were performed on males. ***D,*** Schematic representations of GF circuit outcomes with UAS-*hid*/+ controls and spGal4 10B11-AD ∩ 14A06-DBD driven UAS-*hid* cell ablation. Not pictured are instances where neither GFC1 or PSI are ablated, and instances where both GFIs are absent. ***E,*** Frequency of each GF circuit outcome with the targeted spGal4 10B11-AD ∩ 14A06-DBD driven UAS-*hid* cell ablation. The pie chart color is coded to dots at the bottom of schematics in panel D. The sample size for UAS-*hid*/+ genetic controls is 21 animals, and for the spGal4 cell ablation is 20 animals.

Table 1: Transgenic Gal4 driver lines for the Giant Fiber Circuit

New Gal4 drivers (distinct from those used in this study) that express selectively within the GF circuit, as compiled from the Janelia Flylight and Vienna Tiles library collections.

Selective lines for GFC4 have not been uncovered and thus are not reported here. GFI: Giant Fiber Interneuron, GCI: Giant Commissural Interneuron, TTMn: Tergotrochanteral Motoneuron, PSI: Peripherally Synapsing Interneuron, GFC: Giant Fiber Coupled neurons.

Movie Legends

Movie 1: 3D animation of GFC1 and GFI interaction

Animated 3D reconstruction of mCD8::GFP-labeled GFC1 (green) and TRITC-injected GFI (magenta) in thoracic ganglion segments 1 and 2 (TG1/2). GFC1 intersects with the GFI in a narrow projection that crosses the IB. This projection then splits to create claw-like synaptic terminals in TG1-3 (TG3 not pictured). Scale bar: 20μm.

Movie 2: 3D animation of GFC2 and GFI interaction

Animated 3D reconstruction of mCD8::GFP-labeled GFC2 (green) and TRITC-injected GFI (magenta) in thoracic ganglion segments 1 and 2 (TG1/2). GFC2 extends a large TG2 loop with dorsal projections. GFC2 intersects with the GFI extensively at the IB and to a lesser extent at the tip of the TG2 axonal bend. Scale bar: 20μm.

Movie 3: 3D animation of GFC3 and GFI interaction

Animated 3D reconstruction of mCD8::GFP-labeled GFC3 (green) and TRITC-injected GFI (magenta) in thoracic ganglion segments 2 and 3 (TG2/3). GFC3 cell bodies project processes to the IB and contact the GFI, with extensive branching, including along the GFI axonal bends. GFC3 then projects into TG3 to terminate. Scale bar: 20μm.

Movie 4: 3D animation of GFC4 and GFI interaction

Animated 3D reconstruction of mCD8::GFP-labeled GFC4 (green) and TRITC-injected GFI (magenta) in thoracic ganglion segments 1 and 2 (TG1/2). GFC4 cell bodies project processes from TG1 to the IB, then reverse course and return to TG1 where they terminate. Scale bar: 20μm.

Movie 5: 3D animation of ShakB electrical synapses between GFC1 and GFI at IB

Animated 3D reconstruction of mCD8::GFP-labeled GFC1 (green), TRITC-injected GFI (magenta) and anti-ShakB electrical synapse labeling (cyan). The simple passing dendrite of GFC1 interacts with the GFI at multiple locations within the IB. Multiple sites of ShakB electrical synapses indicate direct GFC1-GFI coupling. Scale bar: 5μm.

Movie 6: 3D animation of ShakB synapses between GFC2 and GFI at IB

Animated 3D reconstruction of mCD8::GFP-labeled GFC2 (green), TRITC-injected GFI (magenta) and anti-ShakB electrical synapse labeling (cyan). The GFC2 field interacts in multiple locations with the GFI, including several side projections from the IB. Several sites of ShakB electrical synapses indicate GFC2-GFI coupling. Scale bar: 5μm.

Movie 7: 3D animation of ShakB synapses between GFC2 and GFI at axonal bend

Animated 3D reconstruction of mCD8::GFP-labeled GFC2 (green), TRITC-injected GFI (magenta) and anti-ShakB electrical synapse labeling (cyan). GFC2 contacts the GFI

along the TG2 axonal bends, mostly at the tips. Along these contact sites there are few to no ShakB contacts (cyan) shared between the neurons. Scale bar: 5μm.

Movie 8: 3D animation of ShakB synapses between GFC3 and GFI at IB

Animated 3D reconstruction of mCD8::GFP-labeled GFC3 (green), TRITC-injected GFI (magenta) and anti-ShakB electrical synapse labeling (cyan). GFC3 extends the largest dendritic field at the IB, with extensive GFC3-GFI contact. Several of these contact points are positive for ShakB electrical synapses. Scale bar: 5μm.

Movie 9: 3D animation of ShakB synapses between GFC3 and GFI at axonal bend

Animated 3D reconstruction of mCD8::GFP-labeled GFC3 (green), TRITC-injected GFI (magenta) and anti-ShakB electrical synapse labeling (cyan). GFC3 extensively contacts the GFI along the GFI axonal bends in TG2. Despite this extensive contact, there are minimal ShakB punctae (cyan) shared between the neurons. Scale bar: 5μm.

Figure 1

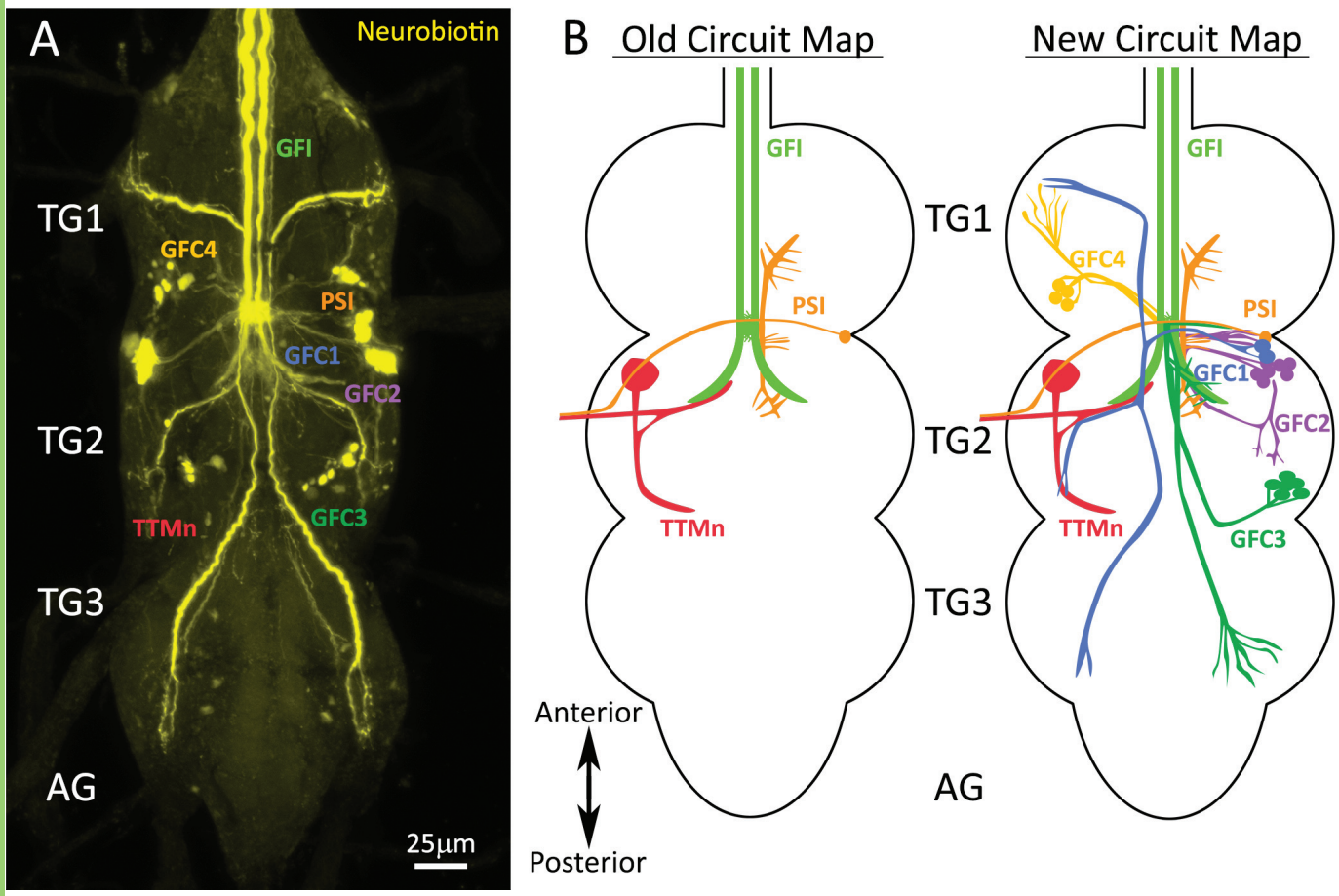

Figure 2

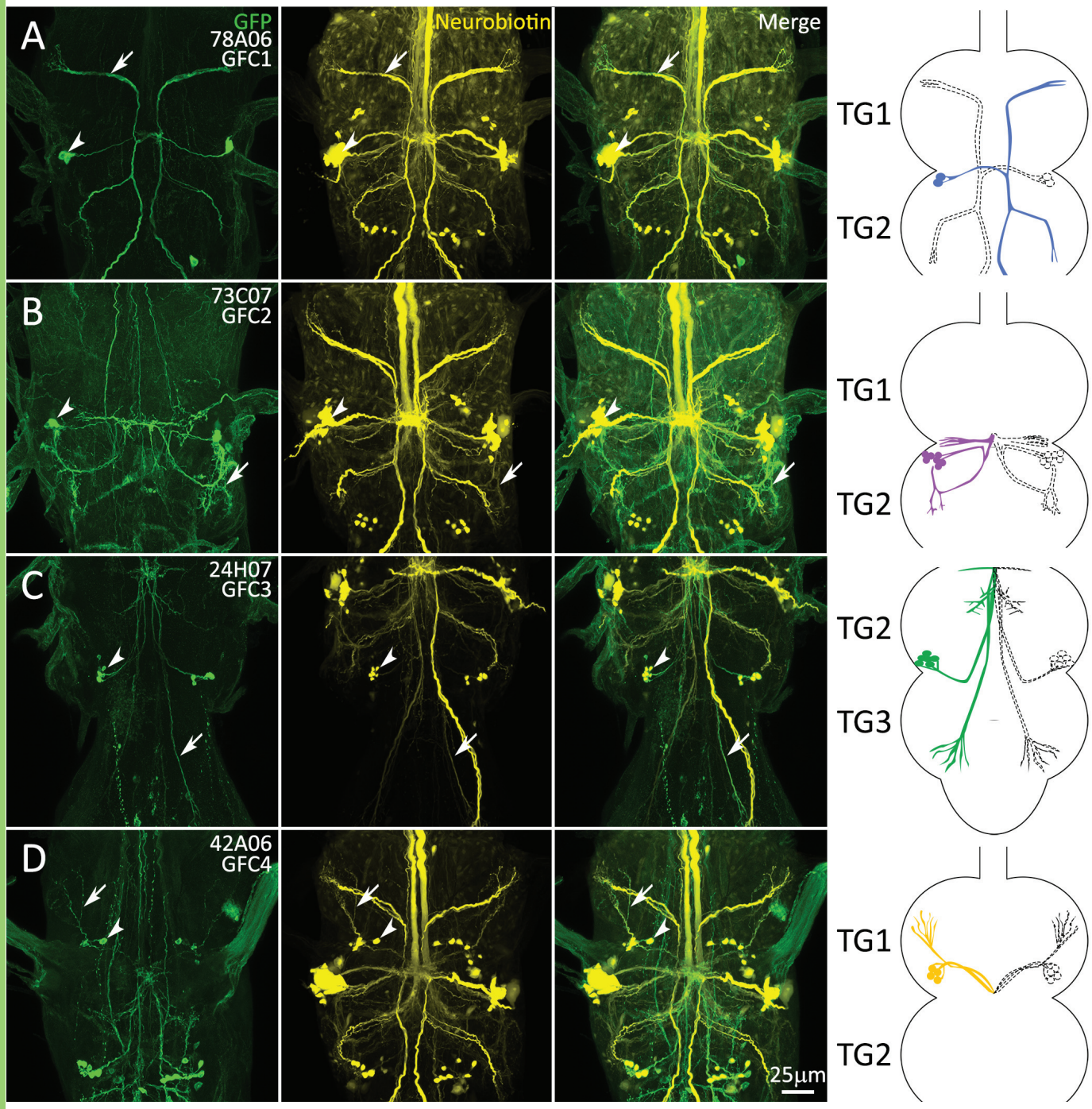

Figure 3

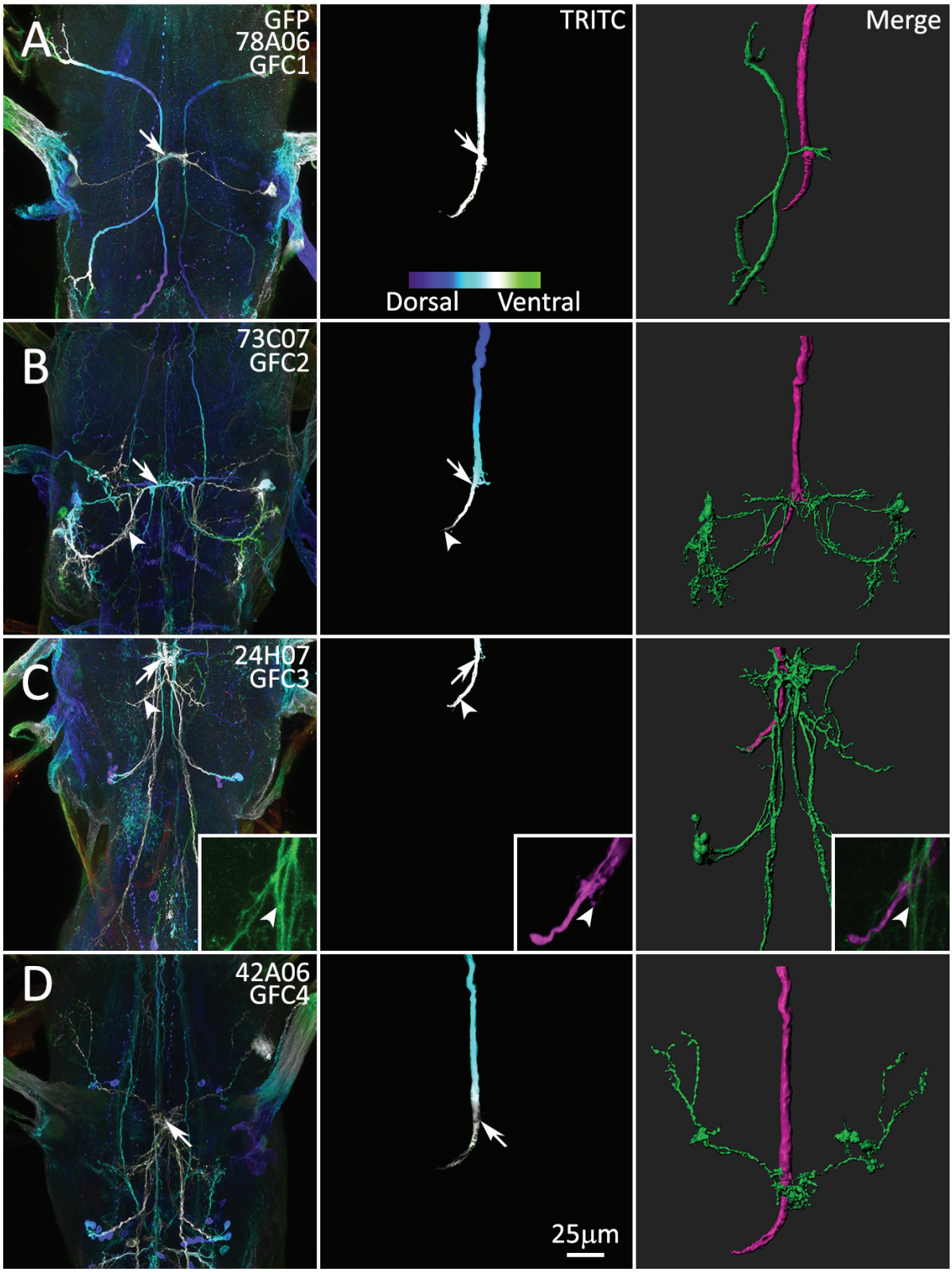

Figure 4

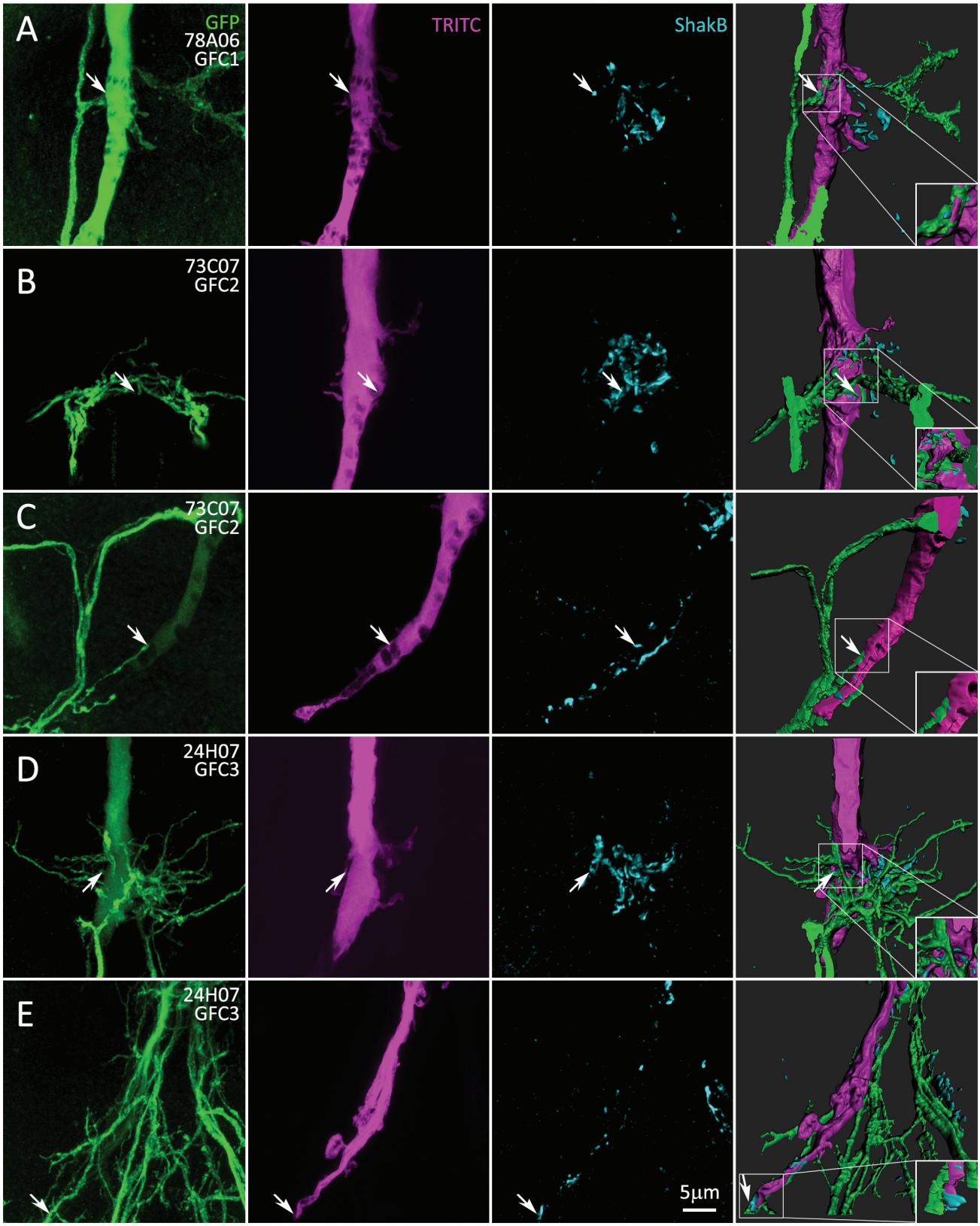

Figure 5

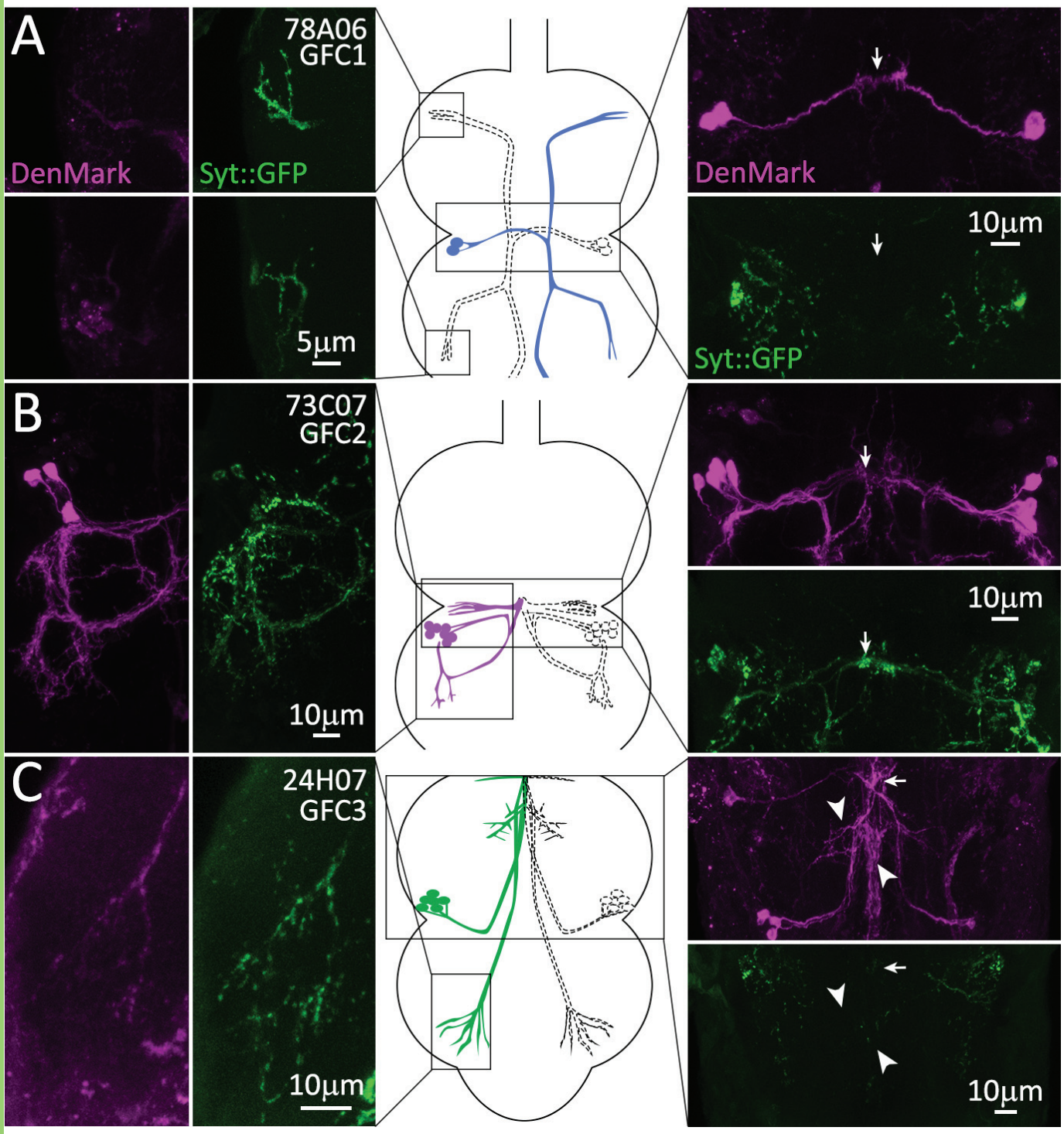

Figure 6

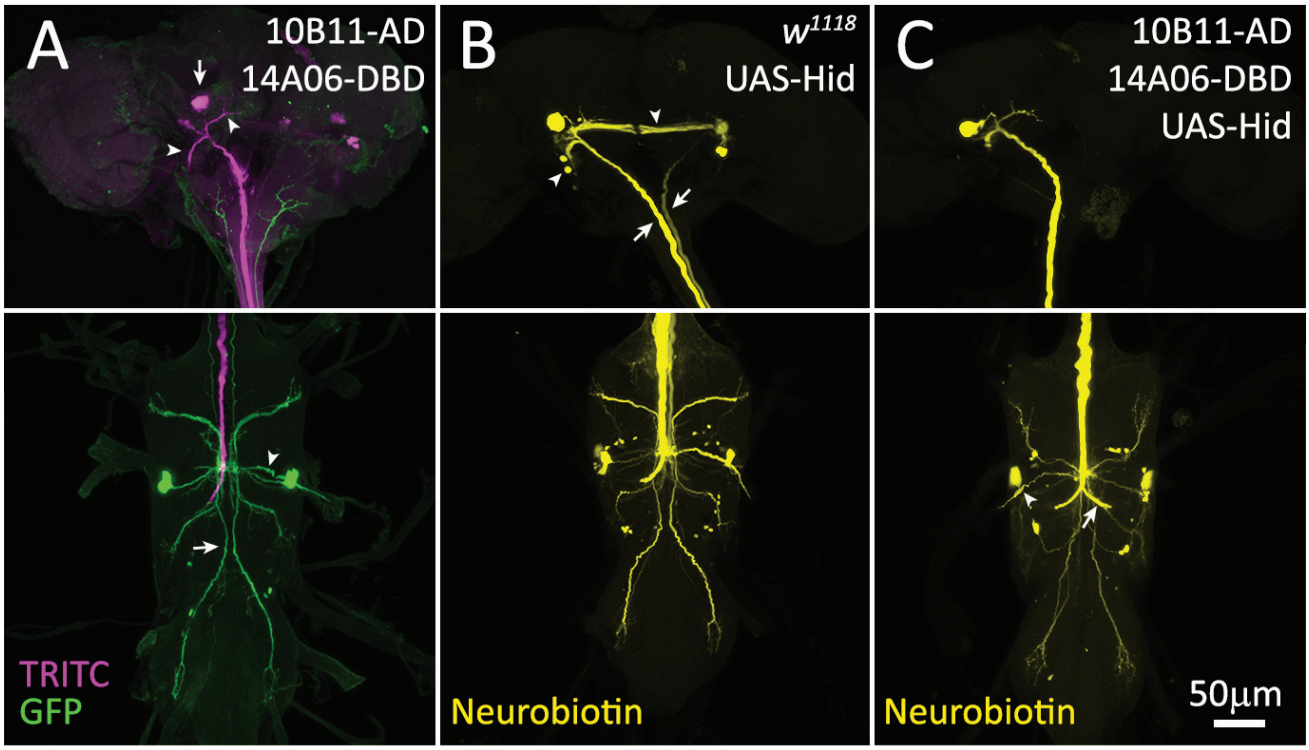

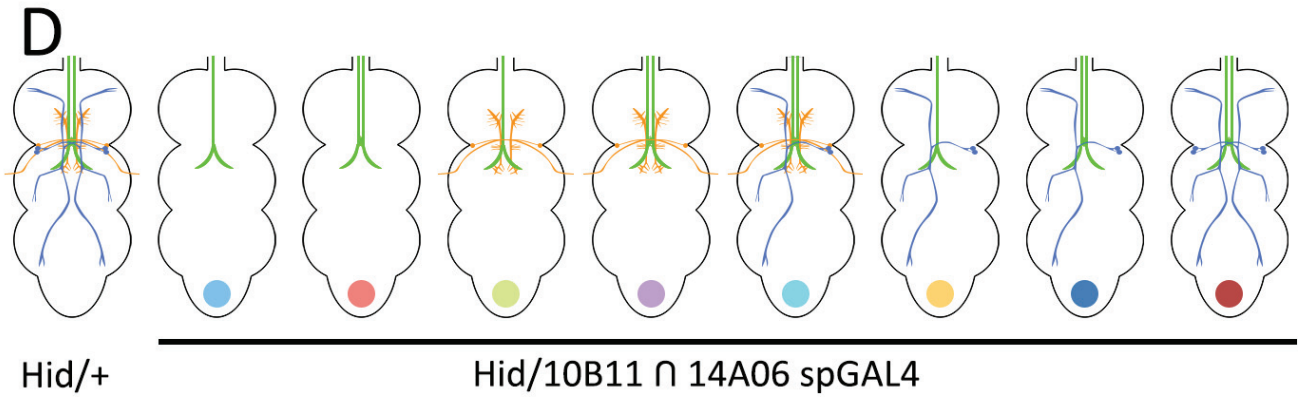

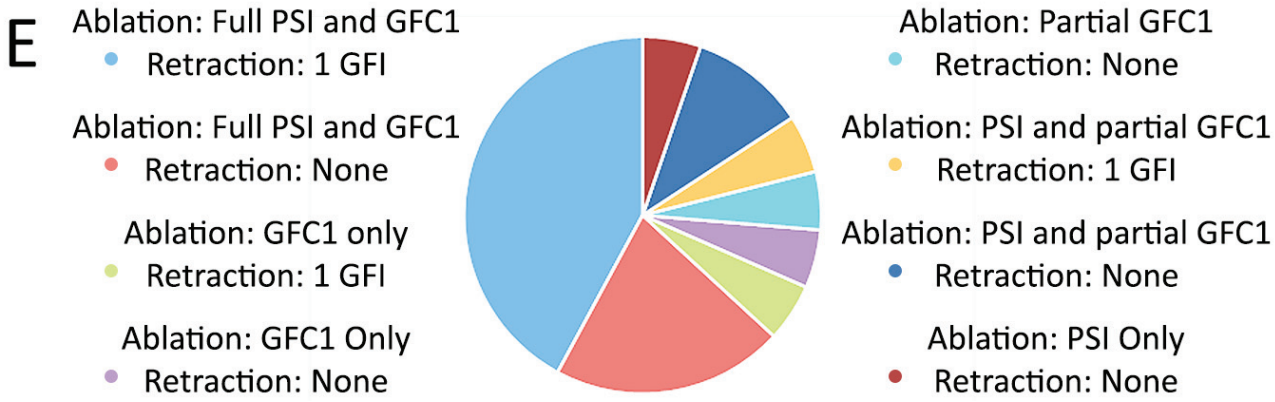

Table 1. Gal4-Driver Lines for the Giant Fiber Circuit

GFI	GCI	TTMn	PSI	GFC1	GFC2	GFC3
R14A01	R32C04	R25D08	R26E04	R93E07	R13C08	R44D02
VT004455	R74E09	R88F07	R75E05	R87D02	R77C12	R58E04
VT042336	VT002209	VT038335	VT030598	VT059438	VT043662	R75D03